Available online at www.sciencedirect.com

ScienceDirect

journal homepage: www.elsevier.com/locate/he

Pd-based membranes performance under hydrocarbon exposure for propane dehydrogenation processes: Experimental and modeling

C. Brencio [a], F.W.A. Fontein [a], J.A. Medrano [a], L. Di Felice [a], A. Arratibel [b], F. Gallucci [a,c,*]

[a] Inorganic Membranes and Membrane Reactors, Chemical Engineering and Chemistry, Eindhoven University of Technology, Eindhoven, the Netherlands

[b] Membrane Technology and Process Intensification / Materials and Processes, TECNALIA, San Sebastian, Spain

[c] Eindhoven Institute for Renewable Energy Systems (EIRES), Eindhoven University of Technology, PO Box 513, Eindhoven 5600 MB, the Netherlands

HIGHLIGHTS

- First investigation of a novel double-skinned PdAg membrane for propane dehydrogenation.
- Transient deactivation trend observed under alkene exposure.
- Development of a 1D model describing concentration polarization and co-adsorption.
- Carbon deposition detected on the selective Pd–Ag layer by preliminary SEM-EDX analysis.

ARTICLE INFO

Article history:
Received 15 April 2021
Received in revised form
25 September 2021
Accepted 29 September 2021
Available online 21 October 2021

Keywords:
Membranes
Membrane reactor
Propane dehydrogenation
Inhibition
Modeling

ABSTRACT

In this work, a novel Pd–Ag double-skinned (DS-) membrane is used for the first time in conditions typical of propane dehydrogenation (PDH). This membrane presents a protective layer on top of the H_2-selective one, which acts as shield against chemical deactivation and mechanical erosion under reaction conditions. While the protective layer is already been proven as an efficient barrier against membrane erosion in fluidized beds, there is no validation yet under PDH reaction. The DS- membrane performance is compared with a conventional (C-) Pd–Ag membrane under alkane/alkene exposure, at 400–500 °C and 3 bar, to investigate whether the incorporation of the protective layer would be suited for H_2 separation in PDH systems, and if coking rate would be affected. The novel membrane shows a H_2 permeance of 2.28×10^{-6} mol·m^{-2} s^{-1}·Pa^{-1} at 500 C and 4 bar of pressure difference, overcoming the performance of the conventional PdAg one ($1.56x \cdot 10^{-6}$ mol m^{-2} s^{-1}·Pa^{-1}). Both membranes present a stable H_2 flux under alkane exposure, while deactivation occurs under exposure to alkenes. A model able to describe the H_2 flux through Pd-based membranes is presented to fit the experimental data and predict membrane performance. The model includes mass transfer limitations in the retentate and a corrective inhibition factor to account for the competitive adsorption of hydrocarbon species in the H_2 selective layer. The experimental results obtained under alkene exposure deviates from model predictions; this can be attributed to carbon

* *Corresponding author*. Inorganic Membranes and Membrane Reactors, Chemical Engineering and Chemistry, Eindhoven University of Technology, Eindhoven, the Netherlands.
E-mail address: F.Gallucci@tue.nl (F. Gallucci).

https://doi.org/10.1016/j.ijhydene.2021.09.252

deposition on the surface of the selective layer, as further detected on the DS-membrane by Scanning Electron Microscopy (SEM)/Energy Dispersive X-Ray Analysis (EDX), which is the main factor for membrane deactivation.

Nomenclature

B_0	Viscous flow parameter [m^2]
C	Molar concentration [mol/m^3]
D_{ij}	Binary diffusion coefficient of component i in component j [m^2/s]
D_{Ki}	Effective Knudsen diffusion coefficient of component i [m^2/s]
d_{pore}	Pore diameter [m]
d_H	Hydraulic diameter [m]
E_a	Activation energy [J/mol]
E_{ads}	Adsorption energy [J/mol]
J_i	Membrane flux of component i [$mol/s/m^2$]
K_i	Adsorption constant of component i [–]
kg	Mass transfer coefficient [m/s]
M_i	Molar mass of component i [kg/mol]
n	Pressure exponent [–]
N_i	Dispersion flux of component i [$mol/s/m^2$]
P	Pressure [Pa]
P_i	Partial pressure of component i [Pa]
Pe	Membrane permeability [mol/s/m]
R	Ideal gas constant [J/mol/K]
Sh	Sherwood number [–]
T	Temperature [K]
x_i	Molar fraction of component i [–]

Greek letters

E	Porosity factor [–]
Δ	Membrane thickness [m]
M	Mean viscosity of binary mixture [Pa s]
T	Tortuosity factor [–]

Introduction

Propylene is one of the main chemicals produced worldwide, as it is used as feedstock for the production of a vast array of chemicals, including polymers (e.g. polyethylene and polypropylene), oxygenates (e.g. propylene oxide and methyl *tert*-butyl ether) and important chemical intermediates (e.g. propionaldehyde). Currently, most of the propylene is obtained as by-product in the naphtha steam cracking process, which aims at ethylene production. Since nowadays the consumption of propylene is growing faster than ethylene, there is the need to find alternative routes that can sustain the global demand of propylene in the coming years [1,2]. The catalytic dehydrogenation of light paraffins into the corresponding olefins is one interesting route already commercialized and installed worldwide, because, being an on-purpose technique, it yields exclusively a particular olefin [3]. More specifically, the direct dehydrogenation of propane leads to propylene, according to the following catalytic reaction:

$$C_3H_8 \leftrightarrow C_3H_6 + H_2 \quad \Delta H_R^{298K} = 120\ kJ/mol$$

These processes can produce olefins of polymer-grade quality. High operating temperatures are required to achieve high conversions, since the dehydrogenation reaction is endothermic and limited by the thermodynamic equilibrium. However, at these temperatures, side cracking reactions are favored and coke is inevitably formed, which rapidly deactivates the catalyst. Therefore, typical operating conditions are in the range of 550–650 °C and low pressures. With these milder conditions the yield is rather low, and thus the separation of the products downstream becomes challenging [4–6]. An interesting strategy to increase the yield of these reactions at lower temperatures is the integration of H_2 selective membranes. The selective removal of H_2 from the catalytic bed shifts the equilibrium beyond the thermodynamic restriction of the conventional process, achieving higher conversions, and consequently reducing the downstream separation efforts [7,8]. Further improvements for the dehydrogenation process can be achieved integrating the membrane module in a fluidized bed reactor; this will provide reduced intra particle mass and heat transfer resistances, better heat management with nearly isothermal operating conditions, and negligible pressure drop [9,10].

Amongst all H_2-selective membranes, palladium-based membranes offer the capacity to extract high fluxes with high perm-selectivities, due to the high permeability of Pd and its alloys (Ag, Cu, Au) for hydrogen [11]. As main drawback, the application of those membranes in dehydrogenation processes is limited by the presence of short chain hydrocarbons and carbon side-products, which may negatively affect the hydrogen flux stability over time. Carbon-based components tend to adsorb on the membrane surface and subsequently dissociate, leading to membrane coking (carbonaceous deposits on the surface), which inhibits the hydrogen adsorption and dissociation, thus reducing its flux [12–15].

Even though the membrane coking has been demonstrated to be reversible through regeneration with diluted oxygen, the large rate of coke formation during dehydrogenation processes limits continuous operation in an integrated membrane reactor. Since the hydrogen flux greatly depends on the Pd-based membrane properties, it is important to investigate various membrane configurations in order to address their resistance to coke formation during dehydrogenation processes. Several

authors have recently studied the permeance inhibition of conventional Pd-alloyed membranes in the presence of light hydrocarbon mixtures. Montesinos et al. [14] analyzed the effects of the composition of propane/propylene mixtures on the hydrogen permeation through commercially available dense Pd–Ag membranes supported on porous stainless steel, while Peters et al. [15] investigated the influence of different alloys, testing the hydrogen flux through conventional unsupported thin Pd–Ag and Pd–Cu alloy films.

In this work, a novel type of Pd-based membrane, double skin Pd–Ag membrane, is investigated under typical dehydrogenation conditions. The difference compared to standard thin film membranes is represented by the presence of an additional ceramic protective layer on top of the selective one, so they have been named double-skinned membranes. These membranes were originally fabricated to resist erosion from the scouring action of the fluidized catalyst, during operation in fluidized bed reactors [16–18]. The protective mesoporous layer makes the membrane more resistant to attrition than a conventional Pd–Ag under fluidization with catalyst particles, showing stable performance for longer time. On the other hand, in a fixed bed reactor the protective layer can shield the selective one from direct contact with the catalyst which could lead to chemical interactions and, as a consequence, membrane deactivation in the long term [17]. Both these aspects are encompassed in this work, since the highly endothermic propane dehydrogenation reaction is conventionally carried out in a catalytic fixed bed, but it can take advantage of the fluidized bed technology. Therefore, it becomes relevant to investigate the performance of this novel membrane and to assess the ability of separating H_2 from propane/propylene mixture without any major drawbacks such as slower molecules diffusion due to increased mass transfer resistance, gas-solid chemical and physical interactions or even clogging of the protective layer due to coke formation.

The performance of the novel double-skinned membrane regarding hydrogen permeation under hydrocarbon exposure and possible coke formation is investigated for the first time in this work. A conventional Pd–Ag alloyed membrane is used as reference. Firstly, a set of characterization tests were conducted to determine the characteristic membrane permeation curves as function of pressure drop, at different temperatures. Afterward, the hydrogen permeation flux was analyzed continuously as function of time under hydrogen-hydrocarbon binary mixtures, at different operating conditions and feed compositions. The experimental results were fitted by a one-dimensional model to provide more insight into the observed effect of hydrocarbon exposure on the membranes performance. Finally, double skinned membrane SEM-EDX characterization after test is presented to confirm the presence of carbon on the Pd–Ag selective layer as deactivating agent.

Experimental materials and methods

Membranes preparation

In this work, two different configurations of Pd-alloyed membranes were analyzed and compared. The membranes were produced following the work of Arratibel at al [18].

Porous tubular substrates made by Al_2O_3 were used as support for producing the Pd-alloyed membranes. The ceramic supports, provided by Rauschert Kloster Veilsdorf, have an asymmetric geometry with external/internal diameter of 14/7 mm and external pore size of 100 nm. According to the procedure reported by Fernandez et al. [19], the porous ceramic tubes were connected to dense ones to guarantee a proper handling of the substrates; subsequently, the co-deposition of the selective Pd–Ag layer was carried out by electroless plating technique (ELP), immersing the tubular support into a plating bath, under same conditions of temperature and reagents reported in a previous work [20]. After the Pd–Ag layer deposition, the samples were cleaned, dried overnight, and annealed at 550 °C for 4 h in a reducing atmosphere (10 vol% H_2 and 90 vol% N_2). One of the two Pd–Ag alloyed (conventional) membranes was turned into a double-skinned membrane, denoted as DS in this work; an additional mesoporous YSZ/γ-Al_2O_3 protecting layer, with pore size of 2–5 nm and containing 50 wt% of YSZ, was deposited on top of the Pd–Ag layer by a dip coating technique at room temperature, resulting in an additional thickness of ~0.5–1 μm. The Pd–Ag composition of the selective layer was determined by measuring the concentration of both metals in the plating bath before and after deposition of the layer, using an ICP-OES technique. The thickness of both ceramic and selective layers was determined by the SEM technique. The selective layer of the double-skinned membrane, containing 6.67 wt% of Ag, has a total thickness of 2–3 μm. On the other hand, the conventional Pd–Ag alloyed membrane, identified as C- in the following sections, has a slightly higher thickness between 3 and 5 μm, with a content of silver equal to 4.23 wt%.

Permeation setup

The supported membranes, with an active length of 80 mm and 136 mm, for the DS- and the C- respectively, were connected to a dense metallic tube on one end and sealed on the other end with a metallic cap using graphite ferrules, following the procedure described by Fernandez at el [19]. Once the sealings were tightened, a leak test was performed at room temperature by feeding helium from the inside of the membranes, while they were submerged in ethanol. No bubbles were detected at a pressure difference of 1 bar across the two sides of the membrane, indicating that the sealings were properly tightened. Finally, the membranes were ready to be tested and they were connected to the flange of the reactor used to perform the experiments.

Prior to investigating the performance of both membranes, they were activated by feeding the reactor with air at 400 °C for 2–3 min, in order to remove possible impurities from the surface.

A schematic representation of the permeation setup used for the gas permeation measurements (single gas and gas mixture tests) can be seen in Fig. 1.

The two membranes were installed in a cylindrical reactor made of stainless steel. The reactor unit was placed in an electrically heated oven where the membranes and the process gases were heated up to the operating temperature. The process gases were regulated by different mass flow controllers, supplied by Brooks Instruments, and fed to the shell

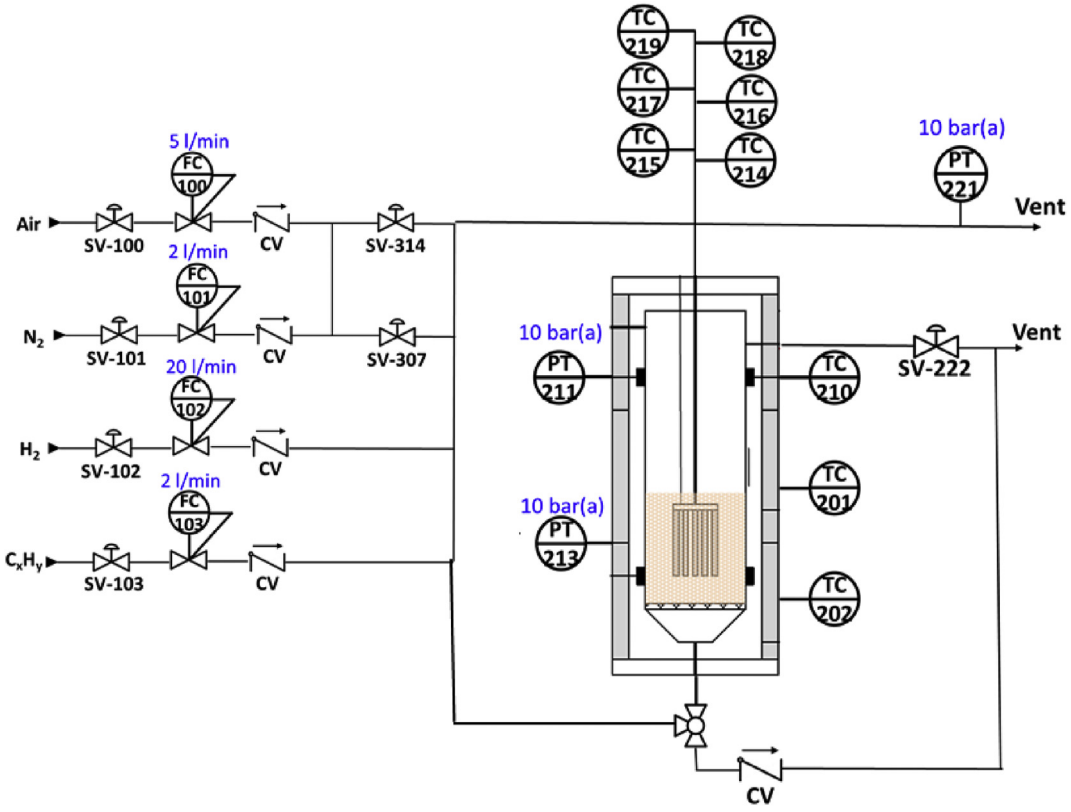

Fig. 1 – Schematic representation of the setup for permeation measurements.

side of the membrane. A back-pressure controller was installed to regulate pressure on the retentate side, while the permeate side of the membrane was kept at atmospheric pressure. An automated soap bubble flow meter from Horibastec, with a measuring range of 2×10^{-3} 10 L/min, was used to measure the amount of permeated gas, separately for each membrane tested.

Single gas permeation tests were carried out at different transmembrane pressure differences, varied from 0.5 to 4 bars, and at temperatures in the range of 400–500 °C, under a pure hydrogen flow. Afterward, binary gas mixture tests were carried out to investigate the effect of hydrocarbons on the H_2 flux through the membrane and the membranes stability. The membranes were cyclically exposed to pure hydrogen and binary (H_2–N_2) or (H_2-C_xH_y) mixtures for a period of time, starting each part of the cycle when the permeation of H_2 was sufficiently stable. To check if the initial hydrogen permeation flux could be recovered after exposure to the hydrocarbon, pure hydrogen was fed in the final step of the cycle. If full recovery of the hydrogen flux was not reached, the membrane was reactivated in air (20 vol% O_2 and 80 vol% N_2) for 2 min, at 400 °C and a total flow rate of 2 l_{STP}/min. Binary gas mixture experiments were conducted at 400 °C, 425 °C and 450 °C, keeping the retentate side at 3 bars and the permeate side at atmospheric pressure, with a total flow rate of 5 L/min. Initially, the molar concentration of hydrogen in the binary mixtures was kept equal to 80%; afterward, to better investigate the effect of exposure to propylene, different hydrogen to hydrocarbon ratios were tested to analyze their influence on the membrane stabilities.

Membrane model description

A one-dimensional model is developed to describe hydrogen flux through Pd–Ag membranes, accounting for mass transfer limitations and competitive adsorption effects, while neglecting coking effects. The model describes the system through linear differential equations along the axial direction of the membrane module, under the assumptions of no radial dispersion and steady state conditions. The solution of the differential equation system has been achieved with Matlab® simulation tool.

Pure hydrogen permeation

To model the hydrogen flux through a Pd-based membrane, an equation written in terms of Richardson equation is applied at each infinitesimal membrane element, as follow:

$$J_{H_2} = \frac{Pe}{\delta}\left(p^n_{H_2\ ret} - p^n_{H_2 perm}\right) \quad (1)$$

where is the membrane permeability, δ is the membrane thickness, $p_{H_2 ret}$ and $p_{H_2 perm}$ are the hydrogen partial pressure at retentate and permeate side, respectively, and n is the exponential factor, which indicates the limiting step of the mechanism by which hydrogen crosses the palladium selective layer. Under the ideal condition of thermodynamic equilibrium between the hydrogen atoms dissolved at the membrane surface and the hydrogen concentration in the gas phase, the pressure exponent n equals to 0.5 and the Richardson

equation (Eq. (1)) takes the form of the so-called Sieverts' law. According to the Sieverts' law (n=0.5), the diffusion of H atoms through the Pd bulk is rate limiting step in the hydrogen permeation mechanism [21–24].

The membrane permeability Pe can be expressed by an Arrhenius-type correlation (Eq. (2)):

$$Pe = Pe_0 \exp\left(-\frac{E_a}{RT}\right) \tag{2}$$

where Pe_0 is the pre-exponential, E_a is the activation energy, R is the universal gas constant and T is the membrane temperature.

Experimental values of pure hydrogen flux for the membranes investigated in this work are used to retrieve the parameters above mentioned, intrinsic of the membrane permeation properties.

Hydrogen permeation in presence of mixtures

When describing the hydrogen permeation from a mixture through a highly selective and permeable membrane (i.e. when the bulk diffusion through palladium is not the only limiting step), a correction of Eq. (1) is required, in order to develop a transport rate expression able to predict several additional effects, which are likely to occur when the membranes are exposed to a mixture of hydrogen and other gases, as reported by many experimental studies [12,14,25]. Those additional effects can be: (i) possible flux decline in the presence of various species due to mass transfer limitation effects; (ii) possible flux decline in the presence of various species due to competitive adsorption; (iii) membrane coking. A detailed description of how mass transfer limitations and competitive adsorption are included in the expression of hydrogen flux is presented in the following sections.

Modeling of mass transfer limitation effects in the retentate side

In presence of mixtures and highly hydrogen permeable membranes, a mass transfer limitation effect in the gas phase, known as concentration polarization, occurs at the retentate side of the membrane. This phenomenon is caused by an accumulation of the non-permeable species and a depletion of hydrogen on the surface of the membrane, leading to a reduction of the hydrogen concentration on the palladium surface compared to the gas bulk. To account for the reduction in hydrogen partial pressure at the retentate side, a correction of the hydrogen flux expression (Eq. (1)) is applied, considering the stagnant-film model for a multicomponent system [10,24]. According to this model, the flux is given by the sum of molecular and convective contributions, as reported in Eq. (3):

$$N_{H_2} = J_{H_2} + x_{H_2} \sum_{i=1}^{N} N_i \tag{3}$$

Substituting the first right term with the corresponding Fick's law and considering only the hydrogen flux, Eq. (3) can be rearranged in Eq. (4):

$$N_{H_2} = \frac{-C_{tot} D_{H_2}}{1 - x_{H_2}} \frac{dx_{H_2}}{dy} \tag{4}$$

Integration of Eq. (4) from the bulk ($y = 0$) to the membrane surface ($y = R^s$), yields to:

$$N_{H_2} = C_{tot} \frac{D_{H_2}}{R^S} \ln\left(\frac{1 - x_{H_2,s}}{1 - x_{H_2,ret}}\right) \tag{5}$$

Considering the mass transfer coefficient from the bulk to the membrane surface, defined as:

$$k_g = \frac{D_{H_2}}{R^S} \tag{6}$$

And rewriting the molar fractions in terms of partial pressures, it is possible to derive from Eq. (5) the following expression:

$$N_{H_2} = C_{tot} k_g \ln\left(\frac{P - P_{H_2,s}}{P - P_{H_2 ret}}\right) \tag{7}$$

The corrected hydrogen partial pressure at the membrane surface ($P_{H_2,s}$), which accounts for the concentration polarization effect, can be obtained by equalizing Eq. (7) with the expression of hydrogen flux through the Pd-based membranes (Eq. (1)), which yields:

$$N_{H_2} = C_{tot} k_g \ln\left(\frac{P - P_{H_2,s}}{P - P_{H_2,ret}}\right) = \frac{Pe}{\delta}\left(P^n_{H_2\ ret} - P^n_{H_2 perm}\right) \tag{8}$$

A Sherwood correlation, available for different velocity and concentration profiles as function of the ratio of annular radii [26], is used to calculate the mass transfer coefficient in the retentate, according to:

$$Sh = \left(k_g \frac{d_H}{D_{H_2}}\right) \tag{9}$$

where d_H is the hydraulic diameter of the reactor, given by the difference between reactor and membrane diameters. It is worth mentioning that this approach is only valid for the conventional Pd–Ag membranes.

When considering the novel double-skinned Pd–Ag membrane, the hydrogen flux experiences an additional resistance at the retentate side of the membrane, due to the presence of the protective porous layer on top of the selective one. This will cause the hydrogen concentration to further decrease from the membrane surface ($r = R^s$) to the interface between the porous layer and the Pd selective layer ($r = R^{int}$), as schematically represented in Fig. 2.

Both molecular friction resistance and support friction resistance are responsible for the mass transfer limitation in the porous protective layer. Such resistances can be estimated according to the dusty-gas model theory, which states that the gas mass transport of H_2 in porous media through a stagnant gas i can be expressed by the following equation [27,28]:

$$-\frac{1}{RT}\frac{dP_{H_2}}{dy} = \frac{1}{D_{KH_2}}\left[J_{H_2} + x_{H_2}\frac{B_0 P}{\bar{\mu} RT}\frac{dP}{dy}\right] + \frac{x_i J_{H_2} - x_{H_2} J_i}{D_{H_2 i}} \tag{10}$$

where the Knudsen diffusion flow (first term), to account for the molecule-pore wall interaction, the viscous flow (second term) and the binary diffusion (third term) are considered.

In Eq. (10), the fluxes of H_2 and the i-species of the binary mixture through a porous media can be expressed according to:

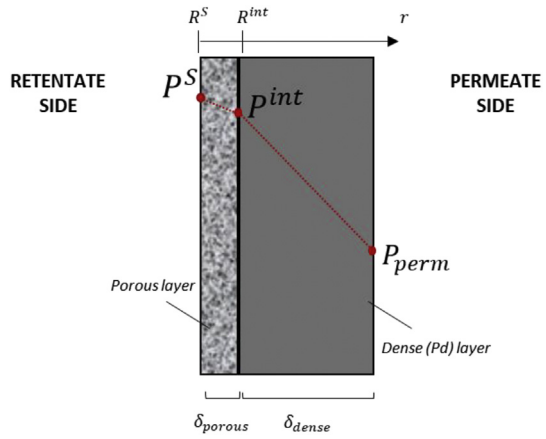

Fig. 2 – Schematic of the double-skinned membrane.

$$J_{H_2} = -\frac{1}{\delta_{porous}} \frac{D_{KH_2}}{RT} \left(1 + \frac{B_0 \overline{P}}{\mu D_{KA}}\right) \frac{dP}{dy} \tag{11}$$

In which:

$$(D_{KA})^{-1} = \frac{x_{H_2}}{D_{KH_2}} + \frac{x_i}{D_{Ki}} \tag{12}$$

Substituting Eq. (11) into Eq. (10) and considering the i-species as stagnant gas ($J_i = 0$), the corresponding Eq. (10) can be integrated in order to obtain the pressure difference across the porous support:

$$\Delta P = P^S - P^{int} = \frac{\ln\left[\frac{1-x_{H_2}^{int}}{1-x_{H_2}^{S}}\right]}{\frac{D_{KH_2}}{D^0_{H_2 i}} + \frac{B_0}{\mu D_{Ki}} + \frac{B_0 D_{KH_2}}{\mu D_{KA} D^0_{H_2 i}} + \frac{1}{\overline{P}}} \tag{13}$$

The effective Maxwell-Stefan gas-gas diffusivity in a porous media is given by:

$$D^0_{H_2 i} = \frac{\varepsilon}{\tau} D_{H_2 i} \tag{14}$$

where ε and τ are the porosity and tortuosity of the ceramic porous layer, respectively.

The effective Knudsen diffusivity is given by:

$$D_{Ki} = \frac{\varepsilon}{\tau} \frac{d_{pore}}{3} \sqrt{\frac{8RT}{\pi M_i}} \tag{15}$$

With d_{pore} being the pore diameter and M_i the molar mass of species i.

The viscous permeability of the porous layer is given by:

$$B_0 = \frac{\varepsilon}{\tau} \frac{d^2_{pore}}{32} \tag{16}$$

In the expressions above, the parameters ε, τ and d_{pore} are respectively the porosity tortuosity and pore diameter of the ceramic porous layer. Those values have been found by fitting the permeation data of the nanoporous YSZ-Al_2O_3 protective layer reported in the work of Alba et al. [29]. The final results obtained are a porosity/tortuosity ratio of 4.2186×10^{-6} and a pore diameter of 3 nm.

In Eq. (13) both the total pressure at the interface (P^{int}) and the hydrogen concentration at the interface ($x^{int}_{H_2}$) are unknown. In order to evaluate these two variables, Eq. (13) can be coupled with the hydrogen flux expression (Eq. (1)) and the Dalton's law:

$$P^{int}_{H_2} = x^{int}_{H_2} P^{int} \tag{17}$$

In this way, it is possible to obtain a system of three equations and three variables, which can be solved applying an iterative procedure proposed by Pinacci et al. [30] and shown in Fig. 3, due to the non-linearity of Eq. (13).

Once the mass transfer limitations in the retentate side have been implemented in the model, considering Eq. (9) for the conventional Pd–Ag membrane, and the combination of Eq. (9) and Eq. (13) for the novel double-skinned Pd–Ag membrane, the model has been validated with experimental values of the hydrogen flux, obtained for binary mixture permeation tests.

Modeling of competitive adsorption effect on membrane surface

In presence of mixtures, the membrane permeance may be inhibited by surface adsorption of other species, reducing the available sites for hydrogen on the PdAg surface and leading to a reduction in the hydrogen flux; this phenomenon has been already observed in several experimental works for carbon monoxide, sulfur, methane, propane and propylene [11,13,14]. However, from a computational point of view, very few studies have addressed this issue, with no available sources of adsorption energies for the gases investigated in this work on the tested membranes.

In order to account for the competitive adsorption of other species during hydrogen permeation through the Pd-based membranes, an inhibition factor is included in the hydrogen flux expression, as stated in Eq. (18) [31]:

$$J_{H_2} = (\theta_V + \theta_H) \frac{Pe}{\delta} \left(p^n_{H_2\ ret} - p^n_{H_2 perm}\right) \tag{18}$$

where θ_V is the fraction of vacant surface adsorption sites, potentially available for hydrogen atoms, and θ_H is the fraction of surface sites already occupied by hydrogen atoms.

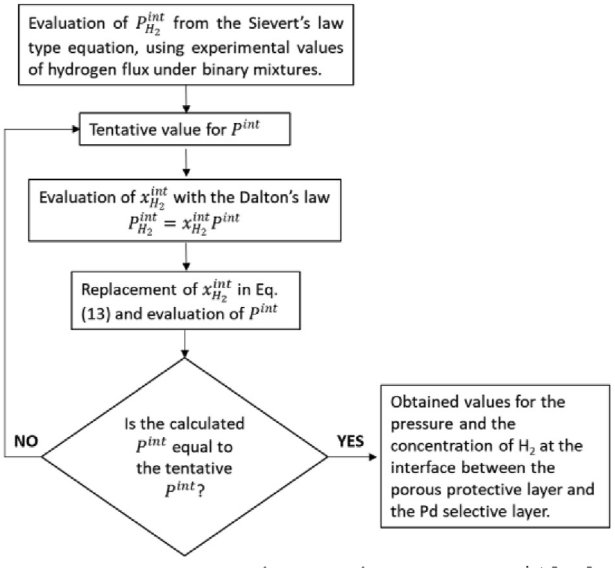

Fig. 3 – Iterative procedure used to compute P^{int} [30].

The inhibition factor is function of the adsorption equilibrium constants of hydrogen and the i-species of the mixtures, of the form:

$$(\theta_V + \theta_H) = \frac{1 + \sqrt{K_H p_H}}{1 + \sqrt{K_H p_H} + \sum_i (K_i p_i)^n} \quad (19)$$

with n representing the number of adsorption sites occupied by the i-species.

The adsorption constant of the i-species (K_i) can be expressed by an Arrhenius type equation of the form:

$$K_i = K_{i0} \exp\left(-\frac{E_{ads}}{RT}\right) \quad (20)$$

The expression for the hydrogen adsorption constant (K_H) on the conventional and novel double-skinned Pd–Ag membranes is calculated from the corresponding pure hydrogen permeation results, following the procedure proposed by Israni et al. [31]. In case of the hydrocarbon species, the pre-exponential factor K_{i0} and adsorption energy E_{ads} of the adsorption equilibrium constants are computed by fitting the experimental values of the hydrogen flux in the binary mixture, at different operating temperatures, with the following rearranged expression of the inhibition factor:

$$(\theta_V + \theta_H) = \frac{J_{H_2,C_x,H_y}|_{\text{experimental}}}{J_{H_2,C_x,H_y}|_{\text{model(only CP)}}} \quad (21)$$

According to Eq. (21), the inhibition factor can be considered as a relative flux; if experimental values of pure hydrogen are considered at the denominator, an overestimation of the relative flux and consequently of the adsorption equilibrium constants is obtained. Indeed, the relative flux with respect to pure hydrogen flux values includes concentration polarization effects due to the hydrocarbon present in the mixture, even if this effect is already accounted in the expression of the hydrogen flux, with the reduced partial pressure of hydrogen on the membrane surface. Expressing the inhibition factor as the relative flux with respect to the flux of hydrogen under hydrocarbon mixture, obtained from the model with only mass transfer limitation effects on the retentate side of the membrane, it was possible to find a better estimation of the adsorption equilibrium constant for the analyzed gases. The values obtained from the fitting are reported in Table 1 per each hydrocarbon species investigated in this work both for the double-skinned and conventional membranes.

Table 1 – Hydrocarbons adsorption equilibrium parameters obtained by fitting experimental results for the DS and C membranes.

Hydrocarbon species	Double-skinned membrane (DS)		Conventional membrane (C)	
	$K_{i0}[-]$	E_{ads}[J/mol]	$K_{i0}[-]$	E_{ads}[J/mol]
C_2H_6	0.0464	52864	0.0124	41319
C_2H_4	0.2335	53903	0.1977	52417
C_3H_8	1.1019	63208	0.8142	60119
C_3H_6	1.6667	63524	1.3633	62584

Results and discussion

Membrane permeation properties: blank tests in H_2 and H_2/N_2

Single gas permeation tests

Pure hydrogen permeation experiments were performed to estimate the pressure exponent n of the power law equation, as reported in Section Pure hydrogen permeation (see Eq. (1)).

The hydrogen permeation for both membranes (DS and C) was measured in a temperature range of 400–500 °C for different transmembrane pressures, after their activation in air.

Fig. 4 shows that the membranes have a linear trend with a pressure exponential factor n (see Eq. (1)) of 0.75 and 0.51 for the DS- and the C- membranes, respectively. Therefore, the best fit for the DS- hydrogen flux is found for an n-value that deviates from the Sieverts law (0.5), indicating that the rate limiting step for the analyzed DS-membrane is not bulk-diffusion, rather it can be attributed to Knudsen diffusion in the mesoporous protective layer [16,32].

Among the two membranes, the double-skinned has better performance, showing a hydrogen permeance of 2.28×10^{-6} mol m^{-2} s^{-1}·Pa^{-1} at 500 °C and a pressure difference of 4 bar, compared to the one of the C- membrane, which is equal to 1.56×10^{-6} mol m^{-2} s^{-1}·Pa^{-1}, under the same operating conditions. This could be related to the fact that the DS-membrane has a thinner selective layer and a higher content of silver on it; as already reported in literature, the addition of Ag to Pd improves the hydrogen permeability, with a 1.7 times larger permeation rate compared to pure palladium [16,33].

Another important parameter to be estimated is the activation energy of Eq. (2), which relates the permeance to temperature according to the Arrhenius relation. The natural logarithm of the calculated permeances was plotted as a function of 1/RT, for the different operating temperatures, and by fitting these data to a linear relationship it was possible to find activation energies and pre-exponential factors for the two membranes, as shown in Fig. 5.

The values found for the activation energy are 7.81 kJ/mol for the double-skinned and 11.21 kJ/mol for the conventional membrane, within the range of reported values for supported Pd-based membranes with similar thickness, ranging from 5.47 to 20.48 kJ/mol [18]. Those values are indicative of the hydrogen permeance in all the different stages of the permeation process, including hydrogen diffusion through the bulk, the selective layer, and the support. The apparent activation energy is therefore dependent on a quite large variety of parameters such as thickness of the membrane, amount of silver in the hydrogen selective layer and the support material. Comparing the values for DS- and C-membranes, the lower activation energy of the DS might be attributed to the fact that the hydrogen must permeate through the mesoporous protective layer in addition to the palladium layer and the support, and this is in agreement with its higher n value discussed above. In the mesoporous protective layer, it is predominant the Knudsen-viscous diffusion mechanism which is typically characterized by

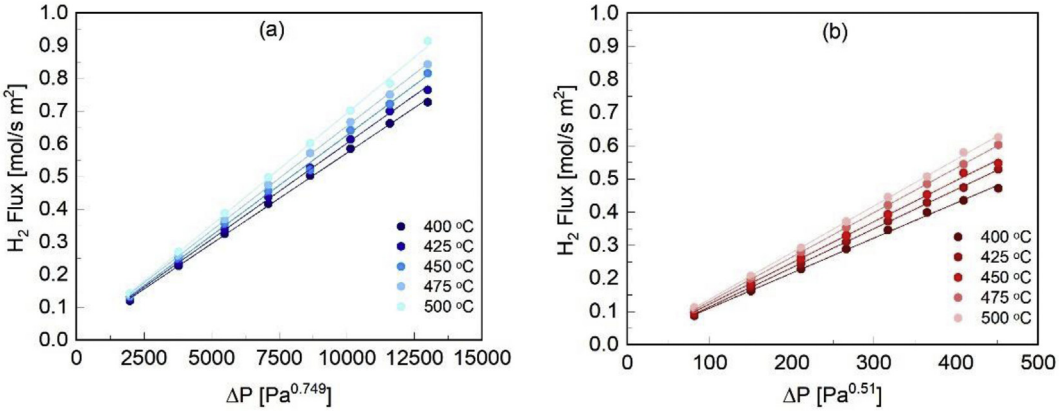

Fig. 4 – Measured hydrogen flux from 400 to 500 °C as a function of the hydrogen partial pressure for the DS (a) and C (b) membranes.

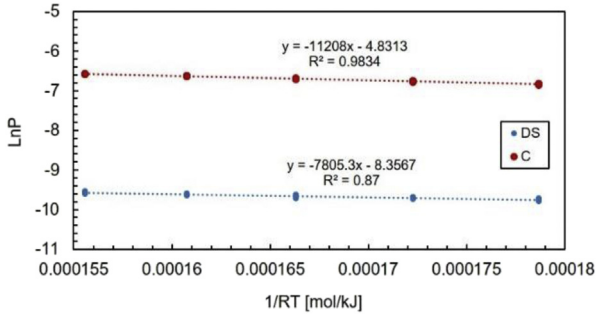

Fig. 5 – Arrhenius plot based on the hydrogen permeance at different T.

lower values of activation energies compared to the solution-diffusion mechanism in the Pd–Ag selective layer [20,34].

H_2/N_2 binary mixture tests

Following the single gas tests, binary mixture tests with hydrogen and nitrogen were performed at 400 °C, 450 °C and 500 °C, keeping a constant 3 bar partial pressure of hydrogen in the feed, atmospheric pressure in the permeate, and with a total feed flow rate of 10 l_{STP}/min. The volume percentage of N_2 in the gas mixture was varied between 10 and 40%. The purpose of these experiments was to investigate the effect of concentration polarization on the hydrogen flux. To measure the effect of the introduction of nitrogen, a relative flux was calculated as the ratio between the flux in the H_2/N_2 case compared to pure hydrogen. The relative fluxes versus the percentage volume fraction of nitrogen are plotted for the two membranes at the above-mentioned temperatures in Fig. 6.

From Fig. 6 it is evident that both membranes suffer from a quite reduced flux even when the ratio of volume of N_2/H_2 is only 10%. At higher operating temperatures, Pd-based membranes are characterized by increased hydrogen fluxes. The higher the amount of hydrogen that permeates, the higher the mass transfer limitation effect. This is shown by the more prominent reduction in the relative flux at higher temperature because of concentration polarization. Even though the DS-membrane has a higher H_2 flux through the thinner selective layer (see Fig. 4), and the additional mesoporous protective layer which increases the mass transfer resistance, its relative flux is only 2% lower than the one measured for the C-membrane. Thus, the concentration polarization experienced by the DS- membrane is comparable to the one of the C-, under the analyzed operating conditions.

Membrane performance in PDH conditions: H_2/C_xH_y mixtures

Several binary mixtures tests were performed to evaluate and compare the behavior of the double-skinned membrane with the conventional Pd–Ag membrane, when exposed to hydrocarbons, both alkanes and alkenes. These alkanes and alkenes are known to be adsorbed on the Pd-based selective surface layer, on which they may dissociate leading to coke formation [14,15]. Therefore, stability tests over time were carried out to address the DS- and C- membranes performance and their resistance towards coke formation, as well as to assess whether or not the addition of the protective layer on the selective one would affect the membrane activity and lifetime during exposure to hydrocarbons. The results are plotted in terms of relative hydrogen flux to allow for a direct comparison of the flux obtained for both membranes under the different operating conditions analyzed. The relative flux corresponds to the measured H_2 flux at each cycle of the test normalized by the flux obtained under pure hydrogen for equal conditions of temperature.

Membrane performance under alkane exposure

The results obtained for binary mixture tests carried out at 400 °C with ethane and propane as hydrocarbons are reported in Fig. 7a and b respectively, for both membranes investigated.

Once steady state values of hydrogen flux were reached for both membranes, after almost 80 min under pure hydrogen exposure, nitrogen was introduced in the mixture with a concentration of 20 vol%. The introduction of nitrogen in the feed mixture leads to the expected reduction in hydrogen flux due to mass transfer limitation (see Section H_2/N_2 binary mixture tests). As soon as the nitrogen is removed, H2 flux is immediately restored. The introduction of C_2H_6 and C_3H_8 in the feed mixture, with a volumetric concentration of 20%, leads to an almost immediate drop in H_2 flux, reaching values lower

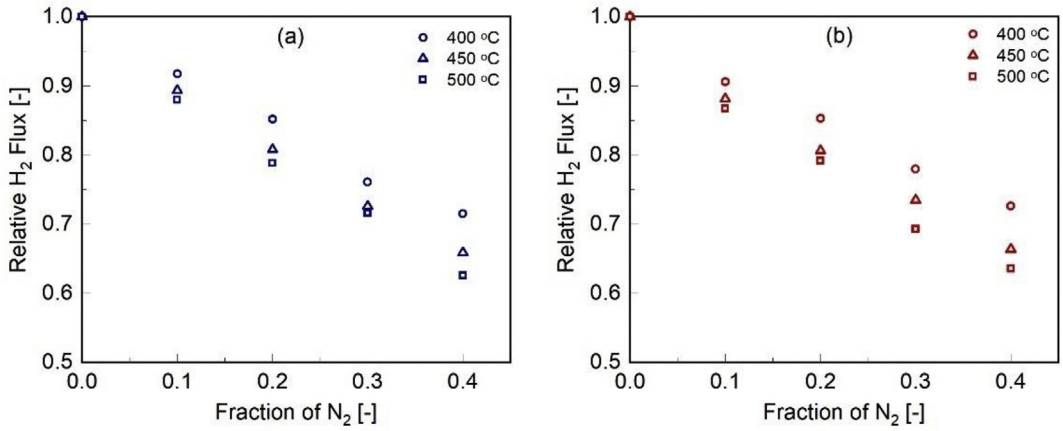

Fig. 6 – Relative H_2 flux as a function of the vol% of N_2 in the binary mixtures at 400 °C, 450 °C and 500 °C, $P_{H2,ret}$ of 3 bar and P_{perm} of 1 bar, for the DS (a) and the C (b) membranes.

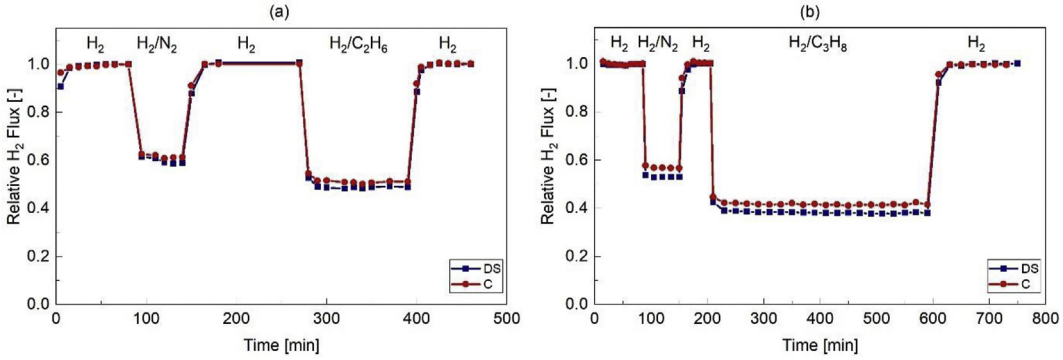

Fig. 7 – Relative H_2 flux in time through the DS and C membranes, under exposure of H_2/C_2H_6 (80/20 vol%) (a) and H_2/C_3H_8 (80/20 vol%) (b), with T = 400 °C, $P_{retentate}$ = 3 bar and $P_{permeate}$ = 1 bar.

than the ones under H_2/N_2 mixture of almost 10% and 15% in case of ethane and propane, respectively. This is explained by the fact that, in case of an alkane, not only concentration polarization is affecting the membrane flux, but also an adsorption of the hydrocarbon molecules on the membrane surface, reducing the available surface sites for hydrogen dissociation. Modeling results confirm this observation (see Section Comparison between experiments and modeling): the flux predicted by the model, when considering only mass transfer limitations on the retentate, is almost 16% and 35% higher than that obtained under competitive adsorption of C_2H_6 and C_3H_8, respectively, for both the C- and DS- membranes. More specifically, in case of the DS- membrane, the model predicts a flux of 0.2378 mol s^{-1} m^{-2}, when only mass transfer resistance in the retentate is described, and a flux of 0.1515 mol s^{-1} m^{-2}, when adding the competitive adsorption, with C_3H_8 in the mixture. However, when removing ethane and propane and continuing the pure hydrogen permeation, a fast and complete recovery of hydrogen flux in the two different membranes is observed. The fact that the hydrogen flux does not decrease over time under alkanes exposure and that it can be fully recovered indicate that the interaction between the alkane and the palladium surface is reversible and it does not lead to coke formation. Thus, it is concluded that in case of exposure to alkanes no major interactions with the protective layer takes place and no coke is formed on it (for DS- membrane) and on the membrane surface (for both C- and DS- membranes).

Membrane performance under alkene exposure

Fig. 8a and b shows the hydrogen flux obtained when exposing the membranes to hydrogen/ethylene and hydrogen/propylene mixtures, respectively; the behavior of the membranes tested is compared at 400 °C and keeping the retentate at 3 bar.

Switching from pure H2 to H2/N2 mixtures results again in an expected drop to steady values of hydrogen flux due to concentration polarization; returning to pure hydrogen the initial flux is restored, as already observed in previous tests. This confirms that the membranes performance is comparable with the previous tests.

When the membranes are exposed to a mixture of 80 vol% H2 and 20 vol% C2H4 (Fig. 8a) a different behavior emerges compared to the hydrogen/alkane mixture. The presence of ethylene leads to a transient decrease in hydrogen flux, which is more evident for the DS- than the conventional C- membrane, with an average deactivation rate of 0.011 and 0.0044 mol m^{-2}·min^{-1}, respectively. This trend indicates that the active hydrogen adsorption sites on the membrane surface are inhibited in the presence of alkene molecules. Moreover, after removal of C2H4 from the feed it is evident that it is not possible to restore the initial performance by feeding pure

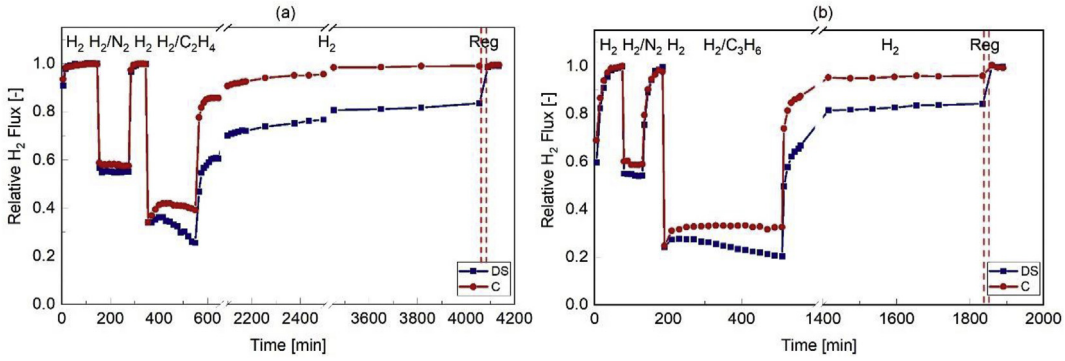

Fig. 8 – Relative H_2 flux in time through the DS and C membranes, under H_2/C_2H_4 (80/20 vol%) (a) and H_2/C_3H_6 (80/20 vol%) (b) exposure, with T = 400 °C, $P_{retentate}$ = 3 bar and $P_{permeate}$ = 1 bar.

hydrogen, with the DS- membrane showing the lowest recovery. After almost 60 h under hydrogen exposure, the DS- membrane can recover 83.5% of its initial flux, compared to the 98% recovery of the C- membrane. This may indicate either that the alkene molecules cannot desorb under the adopted conditions or that their molecular dissociation occurs on the membrane surface under PDH conditions, leading to coke formation.

Similarly, feeding propylene to the membranes leads to a severe decrease in flux (Fig. 8b), with a slightly deactivating trend for the DS- and almost steady state for the C- membrane. After regeneration in H_2 for 20 h, it was possible to recover 84% and 96% of the initial DS- and C- membrane activity, respectively. The lower recovery observed for the DS- membrane under pure H_2 exposure could be explained by an increased coke deposition or adsorption of alkene molecules on the membrane surface – being their removal more difficult due to the presence of the ceramic protective layer.

To restore the initial performance of the membranes it was necessary to reactivate them with air (O_2/N_2: 20/80 vol%) at 400 °C and atmospheric pressure, for 2 min.

It can be concluded that, in both cases of ethylene and propylene dehydrogenation, the presence of the protective layer shows not to play a significant role against deactivation mechanism during exposure to the hydrocarbons, leading to less resiliency to recovery the initial activity under exposure to pure H_2. The main responsible of coke formation due to alkenes dissociation is the metallic membrane surface, rather than the ceramic protective layer as it will be confirmed later by the post characterization results (Section Post characterization).

Effects of operating temperature

Coking effects tend to increase in severity and rate at higher operating temperatures while adsorption generally decreases with temperature [12,35,36]. For this reason, it is likely that coking effects are even more predominantly visible at higher temperatures [15].

Fig. 9a and b summarize the measured hydrogen flux as function of operating temperature, for both the DS- and C- membranes, respectively, under hydrogen/propylene mixture.

The reduction in hydrogen flux becomes more evident at higher operating temperatures, and at 425 °C the transient deactivation trend under exposure to the alkene is experienced even by the C- membrane (Fig. 9b). At 450 °C, both membranes show the most severe deactivation trend, reaching values of hydrogen flux 90% lower than their initial performance with a similar deactivation rate of 0.01 mol/$m^{-2}\cdot min^{-1}$ on average. Moreover, the recovery of the initial activity in pure H_2 (from minute ≈ 600 in both figures) tends to be higher for lower temperatures because of the lower extent of coking on the membranes surface for both the DS and the C membranes. These data confirm that the most predominant mechanism for membrane deactivation at high temperature is carbon formation on the membrane surface rather than adsorption of C3.

Effects of H_2/C_3H_6 ratio

In this section, the coke formation is investigated for different hydrogen to propylene ratios and a comparison of the membrane's behavior is provided. These experiments were conducted at 450 °C since at this temperature the coking effect was observed to be the most predominant.

Fig. 10a and b shows that the hydrogen flux for the different hydrogen to propylene ratios follows similar trends for the analyzed membranes. The ratio between these two gases appears to have a significant influence on the membrane performance. With less than 10 vol% of propylene, the hydrogen flux reaches a steady state quite soon after exposure to the binary mixture. When removing the propylene from the gas mixture, the initial hydrogen flux is obtained quite fast. This indicates that at lower concentrations of alkenes, the mass transfer limitations and reversible interactions between the alkene and the membrane are more predominant than coking. On the contrary, above 10 vol% of propylene, a decrease in hydrogen flux over time is observed, with no possibility of restoring the initial values under pure hydrogen exposure. These decreases are therefore attributed to the decomposition of propylene on the palladium layer of the membranes, resulting in membrane coking.

Comparison between experiments and modeling

The experimental data are compared with modeling results to assess the observation gained analyzing the experimental trends of hydrogen flux under alkane/alkene exposure. The

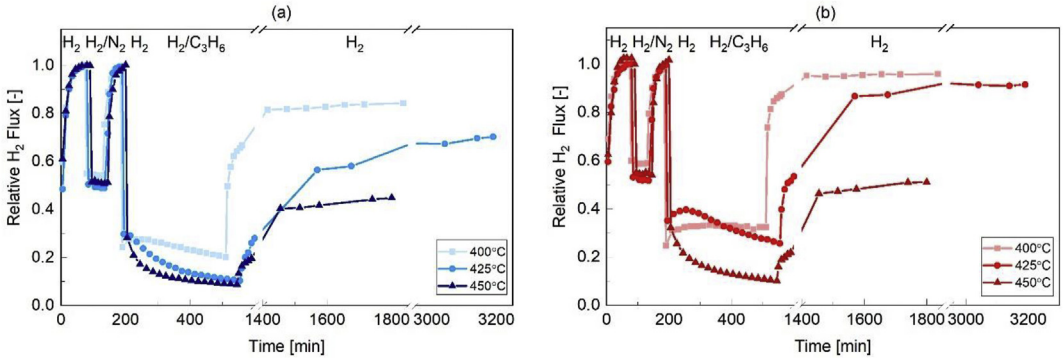

Fig. 9 – Relative H_2 flux in time through the DS (a) and C (b) membranes as function of operating temperature, under H_2/C_3H_6 exposure, with $P_{retentate} = 3$ bar and $P_{permeate} = 1$ bar.

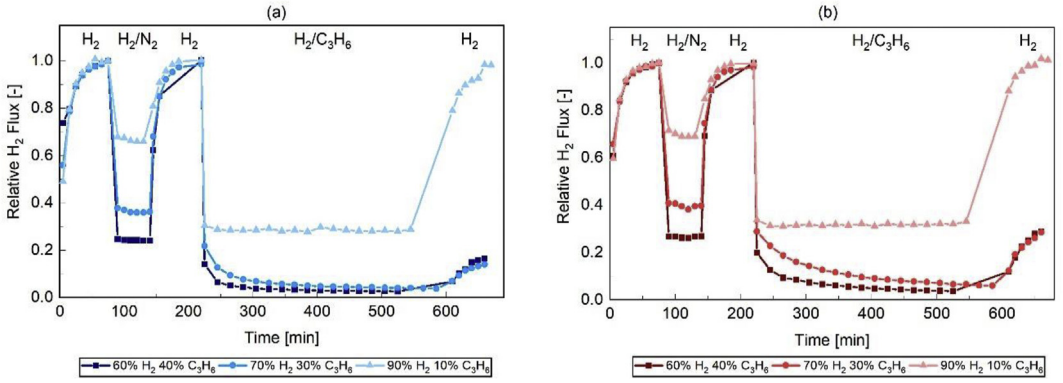

Fig. 10 – H_2 flux in time through the DS (a) and C (b) membranes under H_2/C_3H_6 exposure, at 450 °C, $P_{retentate} = 3$ bar and $P_{permeate} = 1$ bar.

model includes expressions for mass transfer limitation effects on the retentate, accounting for a reduced partial pressure of hydrogen on the membrane surface, and competitive adsorption of the hydrocarbons present in the mixture. This last phenomenon is modelled through adsorption equilibrium constants fitted for the different gases, with values for the pre-exponential factor and adsorption energy reported in Table 1 (see Section Modeling of competitive adsorption effect on membrane surface).

Fig. 11 shows the comparison between experimental data and modeling results obtained for the double-skinned (a) and the conventional Pd–Ag (b) membranes, during H_2–C_2H_6 binary mixture tests at 400 °C.

The values for the pre-exponential factor and adsorption energy of the ethane adsorption equilibrium constant were obtained assuming one adsorption site (n=1) on both membranes. This means that the C_2H_6 molecule makes one adsorption site unavailable for hydrogen according to the following proposed adsorption mechanism (with S being the site):

$$C_2H_6 + S \rightarrow C_2H_6 - S \tag{22}$$

Even if the surface coverage of ethane indicated by the predicted number of adsorption sites is small, the experimental results show that this inhibition effect on hydrogen adsorption, combined with the mass transfer limitation on the membrane bulk, is still rather strong and cannot be neglected. In addition, the higher adsorption energy of ethane on the double-skinned membrane, compared to the one on the Pd–Ag membrane, justifies the bigger drop in hydrogen flux experienced for this membrane.

Fig. 11 shows that the experimental values of hydrogen flux are in good agreement with the model results, when only adsorption mechanisms of the ethane molecule are considered, meaning that no coke is formed on the membrane surface.

When propane is considered, the parameters of the adsorption equilibrium constants for this molecule were obtained considering a number of adsorption sites n equal to 3 on both the DS and the C membranes [36]. The corresponding adsorption mechanism of C_3H_8 molecule is reported below:

$$C_3H_8 + 3S \rightarrow C_3H_8 - S_3 \tag{23}$$

Each molecule of propane blocks 3 adsorption sites for hydrogen, with higher adsorption energies than the one obtained for ethane, as reported in Table 1 (see Section Modeling of competitive adsorption effect on membrane surface).

Thus, propane leads to a higher surface coverage on the Pd-alloyed membranes than the ethane molecule, leading to a stronger inhibition of the hydrogen adsorption. Those observation are in line with the bigger drop in hydrogen flux experienced for H_2/C_3H_8 mixture tests (Fig. 7b). However, also

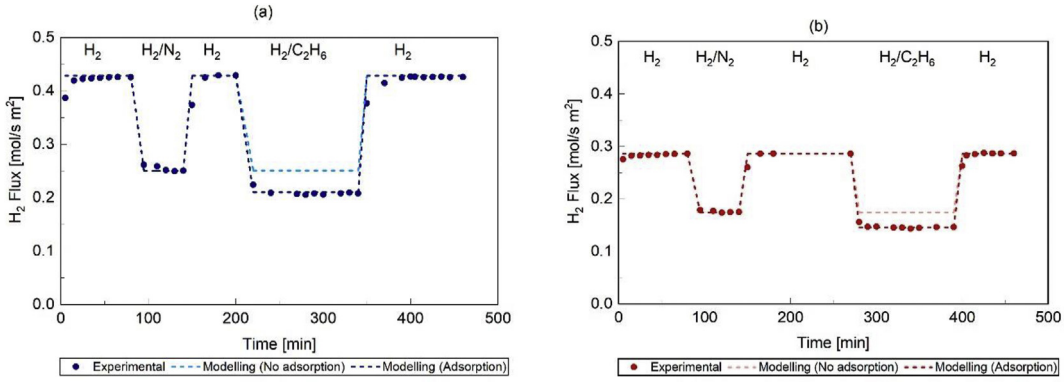

Fig. 11 – Comparison between modeling and experimental results for the hydrogen flux obtained under C_2H_6 exposure, at 400 °C, $P_{retentate}$ = 3 bar and $P_{permeate}$ = 1 bar, for the DS (a) and C (b) membranes.

in case of propane, if only competitive adsorption is considered, the model reproduces the experimental results within a reasonably good accuracy keeping the errors below 5%, for both the membranes simulated, as shown by Fig. 12.

Therefore, it is possible to conclude that the model confirms the absence of coke formation under alkane exposures, providing an accurate fit for the hydrogen flux through the membranes investigated in this work under ethane and propane exposure.

In Fig. 13, the experimental results obtained during H_2–C_2H_4 binary mixture tests at 400 °C are compared with model results for both the double-skinned (a) and the conventional Pd–Ag (b) membranes.

When considering this molecule, the adsorption equilibrium parameters (see Table 1 in Section Modeling of competitive adsorption effect on membrane surface) were obtained by fitting the experimental results with a number of adsorption sites *n* equal to 2 on both membranes. Considering the same surface coverage, the flux inhibition is more evident for the DS- membrane due to the higher adsorption energy compared to the C- membrane. This agrees with the more evident deactivation trend measured experimentally for the DS- than the C- membrane, which cannot be predicted by the model, as shown in Fig. 13a, if only competitive adsorption is considered.

When propylene is considered, the constant values of the adsorption equilibrium constants for this molecule were obtained with a number of adsorption sites *n* equal to 3 on both the DS and the C membranes, as found for propane [36]. The value of adsorption energy obtained for C_3H_6 molecule on the double-skinned and conventional Pd–Ag membranes is slightly higher than the one of C_3H_8, considering the same surface coverage for the two molecules. This implies a higher inhibition of the hydrogen flux due to competitive adsorption. However, in both cases, in presence of the alkene molecule, adsorption is not the only responsible of membrane flux inhibition; as shown by Fig. 14, the flux predicted by the model cannot fit the deactivation trend obtained when feeding H_2/C_3H_6 (min. ≈ 200–600) as well as the permeation values under pure hydrogen flux obtained after the hydrocarbon exposure (min. > 700) – when the membrane is clearly deactivated and does not recover its initial performance.

As a conclusion, under C- and DS- membrane alkene exposures the model is not able to fit experimental data, pointing out coke formation which is not efficiently removed even in the case the alkene is taken off from the mixture (i.e., under pure H_2).

Post characterization

As a final step in the experimental work, a coked double-skinned membrane was analyzed using SEM – EDX analysis in order to detect the presence of coke in the selective and/or in the protective layer. The coking of the membrane was

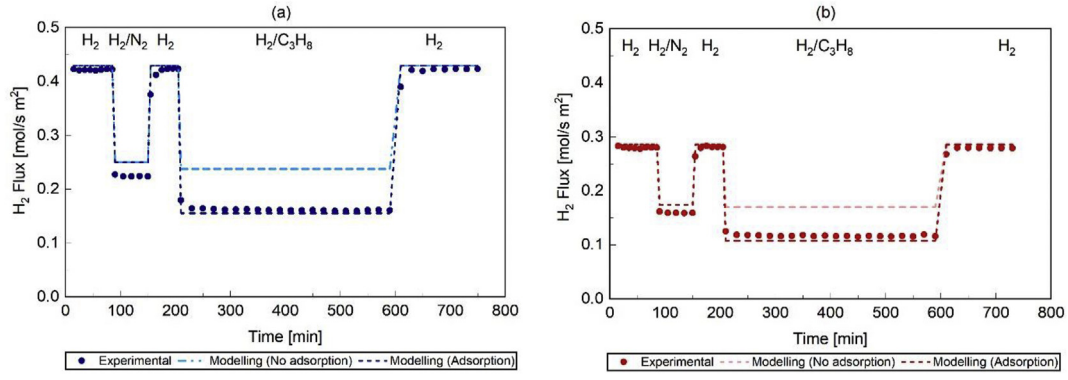

Fig. 12 – Comparison between modeling and experimental results for the hydrogen flux obtained under C_3H_8 exposure, at 400 °C, $P_{retentate}$ = 3 bar and $P_{permeate}$ = 1 bar, for the DS (a) and C (b) membranes.

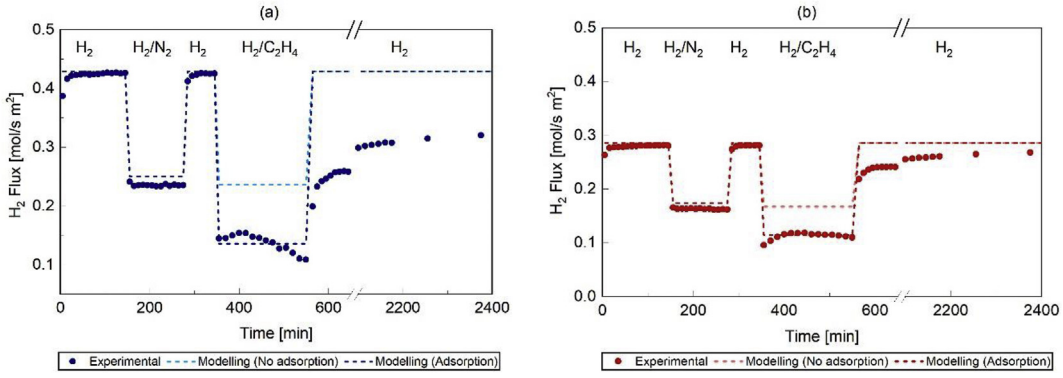

Fig. 13 – Comparison between modeling and experimental results for the hydrogen flux obtained under C_2H_4 exposure, at 400 °C, $P_{retentate}$ = 3 bar and $P_{permeate}$ = 1 bar, for the DS (a) and C (b) membranes.

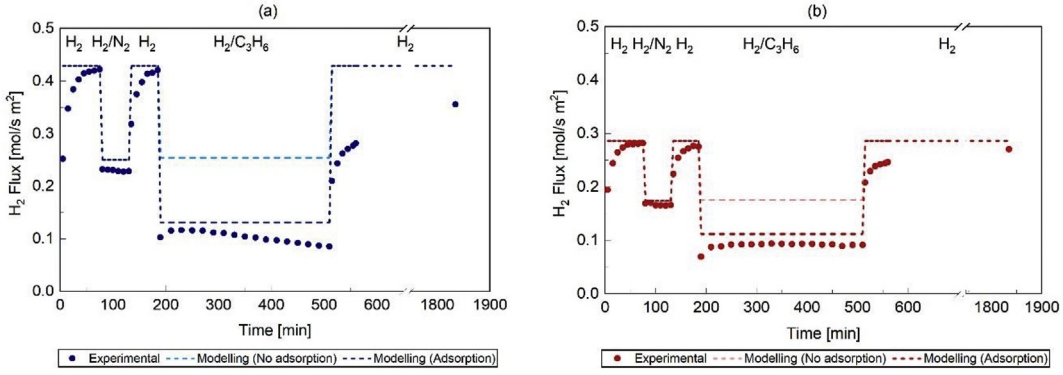

Fig. 14 – Comparison between modeling and experimental results for the hydrogen flux obtained under C_3H_6 exposure, at 400 °C, $P_{retentate}$ = 3 bar and $P_{permeate}$ = 1 bar, for the DS (a) and C (b) membranes.

performed with a H2/C3H6 mixture (60/40 mol%) at 450 °C, keeping the retentate at 3 bar and the permeate at 1 bar, as coking effect was found to be the most severe at these operating conditions in the earlier experiments. The membrane was exposed to these conditions for over 30 h. After this period, the membrane proved to have a severely reduced permeate flow which was also steady over time. Once the double-skinned membrane was removed from the reactor flange, it was prepared to be analyzed as follows. A small piece of membrane was cut, and the dense layer was peeled off from the support to analyze its surface and composition with SEM and EXD.

Two SEM-EDX images are shown for the top layer (protective and selective) of the coked double-skinned membrane. Fig. 15 shows the characterization results of a flawless zone on the top layer (protective ceramic layer); Fig. 16 represents the

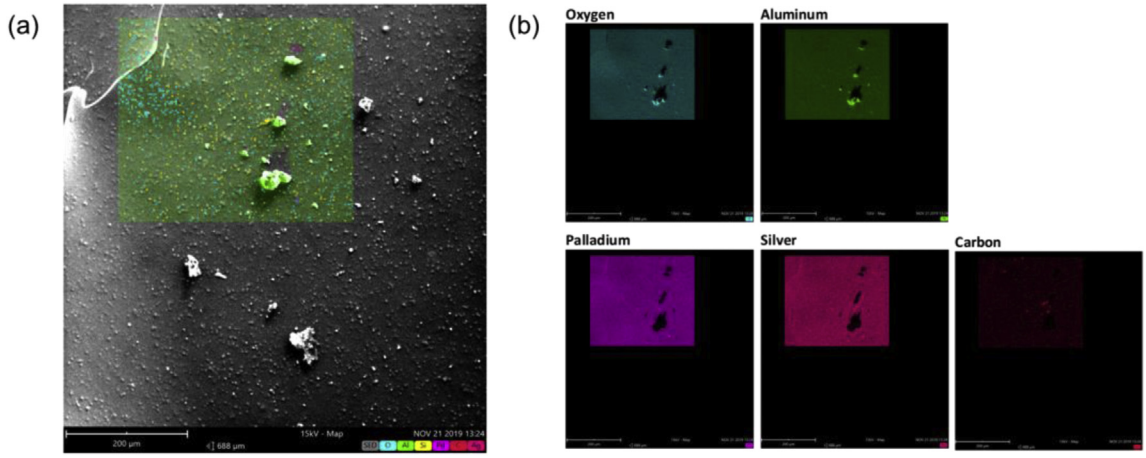

Fig. 15 – SEM (a) and EDX (b) image of the dense layer surface of the coked DS membrane.

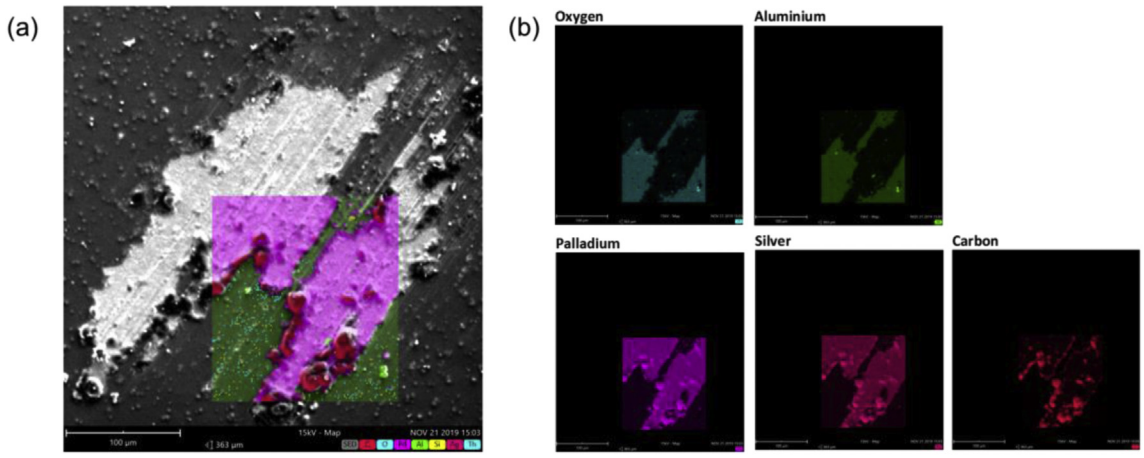

Fig. 16 – SEM (a) and EDX (b) image of the scratched dense layer surface of the coked DS membrane.

results obtained for the dense selective Pd–Ag layer from which the protective layer has been removed during the sample preparation.

In the former, oxygen and aluminum are retrieved over the whole surface with high atomic concentrations, 66% and 14% respectively, as an indication for γ-Al_2O_3, while palladium and silver of the underlying selective layer are detected in lower amounts (5% and 0.8% respectively). In the latter, the darker areas in Fig. 16a mainly consist of oxygen and aluminum, representing the protective ceramic layer. The lighter areas in Fig. 16a show the presence of high concentrations of palladium, silver and carbon (Fig. 16b), representing the hydrogen selective Pd–Ag layer where coke is deposited on. It is worth noticing that carbon is only detected on the edges of the hydrogen selective layer in quite high atomic concentration of around 52%, while it is almost absent on the protective layer of the double-skinned membrane, as shown in Fig. 14b, with a corresponding atomic concentration of 4.2%. It is therefore concluded that coke formation occurs in the Pd–Ag layer and it is more pronounced at its edges. This explains why it is more difficult to regenerate the coked membranes with pure hydrogen in the case of the DS- membrane compared to the other; the hydrogen is more sterically hindered because the coke is less accessible than in the conventional Pd–Ag membrane.

Although this analysis gives some insights on locating the carbon formed on a DS-membrane exposed to PDH reaction conditions, it must be considered as a preliminary investigation, and a more detailed characterization work will be further undertaken.

Conclusions

The behavior of a novel double-skinned membrane for hydrogen separation has been assessed under light hydrocarbon exposure, to evaluate the possible protection to coke formation by the porous layer present on top of the selective substrate. Results in terms of hydrogen flux have been compared with the ones retrieved from a non-protected Pd–Ag membrane, tested simultaneously under same conditions. Several hydrogen/hydrocarbon mixtures were investigated, for both alkanes and alkenes, at different operating temperatures. The experimental results show stable performance for both the double-skinned and the non-protected Pd–Ag membranes under alkanes exposure; the alkanes adsorb on the membrane surfaces with no further decomposition into carbon species and both membranes can restore immediately the initial hydrogen flux as soon as the alkane is removed from the mixture. Under alkenes exposure, a transient deactivation trend of hydrogen flux is observed, due to the decomposition of those molecules on the membrane surfaces. The experimental results are then fitted with a model, developed to describe the hydrogen flux through Pd-based membranes (with and without the protective layer) under concentration polarization and competitive adsorption in binary mixtures. The model predicts well hydrogen fluxes for both membranes in presence of alkane mixtures, while deviates from the experimental results obtained under alkenes exposure. This suggests that the main factor for membrane deactivation under alkene exposure is carbon deposition on the surface of the selective layer, which has been observed by Scanning Electron Microscopy (SEM)/Energy Dispersive X-Ray Analysis (EDX) on the DS-membrane.

Even though the double-skinned membrane shows outstanding H_2 permeances (2.28×10^{-6} mol m^{-2} s^{-1}·Pa^{-1} measured at 500 °C and 4 bar of pressure difference) compared to the conventional one (1.56×10^{-6} mol m^{-2}·s^{-1}·Pa^{-1}), its performance is comparable to the non-protected membrane under alkane/alkene exposure. It seems that the presence of the protective layer does not play a significant role against deactivation mechanism during exposure to the hydrocarbons, and it makes more difficult to recover the initial activity under exposure to pure hydrogen. Nevertheless, this novel double-skinned membrane presents advantages over the conventional PdAg membrane, due to the beneficial effect of the protective layer against mechanical erosion by particle attritions in fluidized beds, which have been already proven for other applications and will be investigated in detail for PDH. Meanwhile, new solutions to improve the resistance to coke formation are

being investigated varying the geometry (pore size distribution) and material composition of the protective layer.

Finally, the kinetics of coke formation on the membrane surface under hydrocarbon exposure will be experimentally investigated to be included in the model for a better prediction of membrane behavior under alkene exposure.

Declaration of competing interest

The authors declare that they have no known competing financial interests or personal relationships that could have appeared to influence the work reported in this paper.

Acknowledgments

This project has received funding from the European Union's Horizon 2020 research and innovation program under grant agreement No 814671 (BiZeolCat).

REFERENCES

[1] Sattler JJHB, Ruiz-Martinez J, Santillan-Jimenez E, Weckhuysen BM. Catalytic dehydrogenation of light alkanes on metals and metal oxides. Chem Rev 2014;114(20):10613–53.
[2] Agarwal A, Sengupta D, El-Halwagi M. Sustainable process design approach for on-purpose propylene production and intensification. ACS Sustain Chem Eng 2018;6(2):2407–21.
[3] Nawaz Z. Light alkane dehydrogenation to light olefin technologies: a comprehensive review. Rev Chem Eng 2015;31(5).
[4] Lobera MP, Téllez C, Herguido J, Menéndez M. Transient kinetic modelling of propane dehydrogenation over a Pt-Sn-K/Al2O3 catalyst. Appl Catal A Gen 2008;349(1–2):156–64.
[5] Li Q, Sui Z, Zhou X, Chen D. Kinetics of propane dehydrogenation over Pt-Sn/Al2O3 catalyst. Appl Catal A Gen 2011;398(1–2):18–26.
[6] Zangeneh FT, Taeb A, Gholivand K, Sahebdelfar S. Kinetic study of propane dehydrogenation and catalyst deactivation over Pt-Sn/Al2O3 catalyst. J. Energy Chem. 2013;22(5):726–32.
[7] Gallucci F, Fernandez E, Corengia P, Van Sint M. Recent advances on membranes and membrane reactors for hydrogen production. Chem Eng Sci 2013;92:40–66.
[8] Ricca A, Montella F, Iaquaniello G, Palo E, Salladini A, Palma V. Membrane assisted propane dehydrogenation: experimental investigation and mathematical modelling of catalytic reactions. Catal Today 2019;331(June):43–52.
[9] Medrano JA, Julián I, Herguido J, Menéndez M. Pd-Ag membrane coupled to a two-zone fluidized bed reactor (TZFBR) for propane dehydrogenation on a Pt-sn/MgAl2O4 catalyst. Membranes 2013;3(2):69–86.
[10] Helmi A, Fernandez E, Melendez J, Tanaka DAP, Gallucci F, Van Sint Annaland M. Fluidized bed membrane reactors for ultra pure H2 production - a step forward towards commercialization. Molecules 2016;21(3).
[11] de Nooijer N, et al. Influence of H2S on the hydrogen flux of thin-film PdAgAu membranes. Int J Hydrogen Energy 2020;45(12):7303–12.
[12] Gallucci F, Chiaravalloti F, Tosti S, Drioli E, Basile A. The effect of mixture gas on hydrogen permeation through a palladium membrane: experimental study and theoretical approach. Int J Hydrogen Energy 2007;32(12):1837–45.
[13] Jung SH, Kusakabe K, Morooka S, Kim S-D. Effects of co-existing hydrocarbons on hydrogen permeation through a palladium membrane. J Membr Sci 2000;170(1):53–60.
[14] Montesinos H, Julián I, Herguido J, Menéndez M. Effect of the presence of light hydrocarbon mixtures on hydrogen permeance through Pd-Ag alloyed membranes. Int J Hydrogen Energy 2015;40(8):3462–71.
[15] Peters TA, Liron O, Tschentscher R, Sheintuch M, Bredesen R. Investigation of Pd-based membranes in propane dehydrogenation (PDH) processes. Chem Eng J 2016;305:191–200.
[16] Arratibel A, Medrano JA, Melendez J, Pacheco Tanaka DA, van Sint Annaland M, Gallucci F. Attrition-resistant membranes for fluidized-bed membrane reactors: double-skin membranes. J Membr Sci 2018;563:419–26.
[17] Arratibel A, Pacheco Tanaka A, van Sint Annaland M, Gallucci F. On the use of double-skinned membranes to prevent chemical interaction between membranes and catalysts. Int J Hydrogen Energy 2019;(xxxx).
[18] Arratibel A, Pacheco A, Laso I, Van Sint M. Development of Pd-based double-skinned membranes for hydrogen production in fl uidized bed membrane reactors. J Membr Sci 2018;550:536–44. October 2017.
[19] Fernandez E, et al. Development of thin Pd-Ag supported membranes for fluidized bed membrane reactors including WGS related gases. Int J Hydrogen Energy 2015;40(8):3506–19.
[20] Arratibel A, Antonio J, Melendez J, Pacheco DA. Attrition-resistant membranes for fl uidized-bed membrane reactors : double- skin membranes. J Membr Sci 2018;563(April):419–26.
[21] Bellini S, Azzato G, Gallucci F, Caravella A. "3: mass transport in hydrogen permeation through Pd-based membranes," in current Trends and future Developments on (bio-) membranes. Elsevier Inc.; 2020. p. 63–90.
[22] De Falco M. Membrane reactors modeling. 2011. p. 79–102.
[23] Melendez J, Fernandez E, Gallucci F, Van Sint M, Arias PL, Pacheco DA. Preparation and characterization of ceramic supported ultra-thin (~ 1 μm) Pd-Ag membranes. J Membr Sci 2017;528(January):12–23.
[24] Nordio M, et al. Effect of sweep gas on hydrogen permeation of supported Pd membranes: experimental and modeling. Int J Hydrogen Energy 2019;44(8):4228–39.
[25] Murmura MA, Sheintuch M. Permeance inhibition of Pd-based membranes by competitive adsorption of CO : membrane size e ff ects and fi rst principles predictions. Chem Eng J 2018;347(April):301–12.
[26] Boon J, Li H, Dijkstra JW, Pieterse JAZ. 2-Dimensional membrane separator modelling: mass transfer by convection and diffusion. Energy Procedia 2011;4:699–706.
[27] Veldsink JW, van Damme RMJ, Versteeg GF, van Swaaij WPM. The use of the dusty-gas model for the description of mass transport with chemical reaction in porous media. Chem Eng J Biochem Eng J 1995;57(2):115–25.
[28] Ünal A. Gaseous mass transport in porous media through a stagnant gas. Ind Eng Chem Res 1987;26(1):72–7.
[29] Arratibel A, Astobieta U, Alfredo D, Tanaka P, Van Sint M, Gallucci F. N 2 , He and CO 2 diffusion mechanism through nanoporous YSZ/g -Al 2 O 3 layers and their use in a pore-filled membrane for hydrogen membrane reactors. Int J Hydrogen Energy 2015;41(20):8732–44.
[30] Pinacci P, Drago F. Influence of the support on permeation of palladium composite membranes in presence of sweep gas. Catal Today 2012;193(1):186–93.

[31] Israni SH, Harold MP. Methanol steam reforming in Pd-Ag membrane reactors: effects of reaction system species on transmembrane hydrogen flux. Ind Eng Chem Res 2010;49(21):10242–50.
[32] Shao C-T, Lang W-Z, Yan X, Guo Y-J. Catalytic performance of gallium oxide based-catalysts for the propane dehydrogenation reaction: effects of support and loading amount. RSC Adv 2017;7(8):4710–23.
[33] Basile A, Iulianelli A, Longo T, Liguori S, De Falco M. Membrane reactors for hydrogen production processes. 2011.
[34] Gielens FC, Tong HD, Vorstman MAG, Keurentjes JTF. Measurement and modeling of hydrogen transport through high-flux Pd membranes, vol. 289; 2007. p. 15–25.
[35] Unemoto A, Kaimai A, Sato K, Otake T, Yashiro K. Surface reaction of hydrogen on a palladium alloy membrane under, vol. 32; 2007. p. 4023–9.
[36] Abir H, Sheintuch M. Modeling H2 transport through a Pd or Pd/Ag membrane, and its inhibition by co-adsorbates, from first principles. J Membr Sci 2014;466:58–69.